CHEMISTRY OF MATERIALS
Cite This: Chem. Mater. 2018, 30, 1566−1574
Article
pubs.acs.org/cm

Selective Hydride Occupation in $BaVO_{3-x}H_x$ ($0.3 \leq x \leq 0.8$) with Face- and Corner-Shared Octahedra

Takafumi Yamamoto,[†] Kazuki Shitara,[‡,§] Shunsaku Kitagawa,[∥] Akihide Kuwabara,[§] Masahiro Kuroe,[†] Kenji Ishida,[∥] Masayuki Ochi,[⊥] Kazuhiko Kuroki,[⊥] Kotaro Fujii,[∇] Masatomo Yashima,[∇] Craig M. Brown,[#] Hiroshi Takatsu,[†] Cedric Tassel,[†] and Hiroshi Kageyama*[,†,^]

[†]Department of Energy and Hydrocarbon Chemistry, Graduate School of Engineering, Kyoto University, Nishikyo-ku, Kyoto 615-8510, Japan

[‡]Center for Materials Research by Information Integration (CMI2) Research and Services Division of Materials Data and Integrated System (MaDIS), National Institute for Materials Science (NIMS), Tsukuba, Ibaraki 305-0047, Japan

[§]Nanostructures Research Laboratory, Japan Fine Ceramics Center, Nagoya 456-8587, Japan

[∥]Department of Physics, Graduate School of Science, Kyoto University, Kyoto 606-8502, Japan

[⊥]Department of Physics, Osaka University, Toyonaka, Osaka 560-0043, Japan

[∇]Department of Chemistry, School of Science, Tokyo Institute of Technology, Tokyo 152-8551, Japan

[#]Center for Neutron Research, National Institute of Standards and Technology, Gaithersburg, Maryland 20899, United States

[^]CREST, Japan Science and Technology Agency (JST), Kawaguchi, Saitama 332-0012, Japan

Supporting Information

ABSTRACT: A growing number of transition metal oxyhydrides have recently been reported, but they are all confined to perovskite-related structures with corner-shared octahedra. Using high pressure synthesis, we have obtained vanadium oxyhydrides $BaVO_{3-x}H_x$ ($0.3 \leq x \leq 0.8$) with a 6H-type hexagonal layer structure consisting of face-shared as well as corner-shared octahedra. Synchrotron X-ray and neutron diffraction measurements revealed that, in $BaVO_{2.7}H_{0.3}$, H^- anions are located selectively at the face-shared sites, as supported by DFT calculations, while $BaVO_{2.2}H_{0.8}$ contains H^- anions at both sites though the face-shared preference is partially retained. The selective hydride occupation for $BaVO_{2.7}H_{0.3}$ appears to suppress electron hopping along the *c* axis, making this material a quasi-two-dimensional metal characterized by anomalous temperature dependence of the electrical resistivity and strong antiferromagnetic fluctuations. In contrast, the anion disordered $BaVO_{3-x}H_x$ in hexagonal ($x \approx 0.8$) and cubic ($x \approx 0.9$) forms exhibits a semiconducting behavior. This study offers a wide opportunity to develop transition metal oxyhydrides having various polyhedral linkages, along with site preference of H/O anions, aimed at finding interesting phenomena.

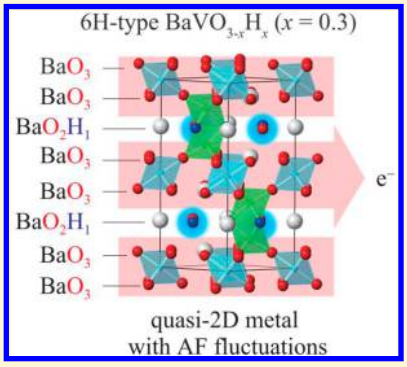

1. INTRODUCTION

Oxyhydrides, where a transition metal (M) center is coordinated to both oxide (O^{2-}) and hydride (H^-) ligands, have recently been developed as a new class of mixed-anion system, with a series of unprecedented chemical and physical properties that are not accessible in simple oxides. For example, the hydride anion is lighter in mass, is smaller in charge (cf. the oxide anion), and has a high standard potential of −2.2 V for H^-/H_2, which makes this ligand mobile and labile. The lability of the hydride in $ATi(O,H)_3$ (A = Ba, Sr, and Eu;[1−3] Figure 1a) allows topochemical anion exchange reactions to occur, leading to novel mixed-anion compounds such as $ATi(O,N)_3$ oxynitrides exhibiting ferroelectricity[4] and $SrTi(O,H,OH)_3$ with H^- and H^+ ions coexisting in the perovskite lattice.[5]

Another important feature of hydride anions that differentiates them from any other anions (O^{2-}, F^-, N^{3-}, etc.) lies in its outermost shell that consists of 1s orbitals. The lack of p orbitals in H^- bestows important consequence in magnetic interactions and resultant physical properties. $SrVO_2H$ (V^{3+}; d^2) with hydride anions at the apical site is a quasi-two-dimensional (2D) Mott insulator with anisotropic magnetic interactions (Figure 1b);[6] The V−H−V interaction along the *c* axis is much weaker than the V−O−V one in the *ab* plane owing to the orthogonal arrangement between V t_{2g} and H 1s orbitals.[7,8] Furthermore, a pressure-induced metallic phase was found to be of 2D nature, indicating that H^- can effectively blocks the interactions along the *c* axis.[9] By contrast, $LaSrCoO_3H_{0.7}$ ($Co^{1.7+}$; $d^{7.3}$) has strong σ-bonding of Co e_g and H 1s orbitals (Figure 1c), which gives rise to a high magnetic order temperature.[10,11]

Received: October 31, 2017
Revised: February 10, 2018
Published: February 12, 2018

© 2018 American Chemical Society

DOI: 10.1021/acs.chemmater.7b04571
Chem. Mater. 2018, 30, 1566−1574

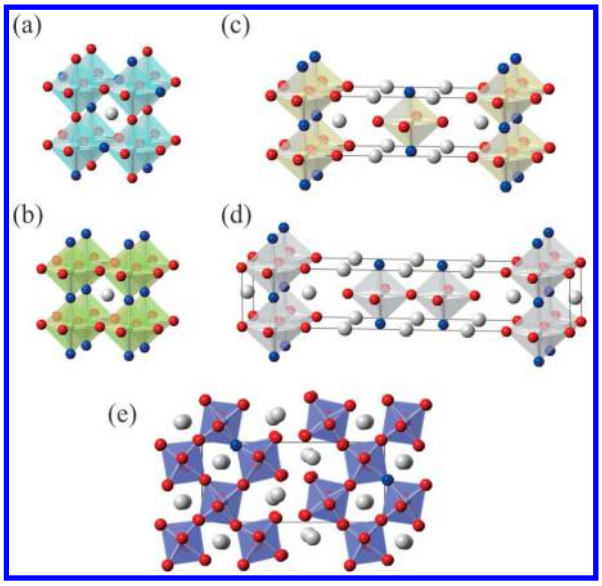

Figure 1. Reported transition metal oxyhydrides, where gray, red, and blue spheres represent A, O, and H atoms, respectively, and transition metal cations lie in the octahedral center. Perovskite structures with (a) anion disorder (e.g., $ATiO_{3-x}H_x$[1]) and (b) anion order ($SrVO_2H$[6]). RP-type perovskites with (c) single octahedral layers (e.g., Sr_2VO_3H[6] and $LaSrCoO_3H_{0.7}$[10]) and (d) double octahedral layers (e.g., $Sr_3V_2O_5H_2$[6]), along $[001]_p$. (e) $La_2Ti_2O_{6.73}H_{0.02}$ with octahedral layers along $[110]_p$.[16] Note that a partial anion order is observed in $LaSrMnO_{3.3}H_{0.7}$[14] (c) and $Sr_3Co_2O_{4.33}H_{0.84}$[17] (d). All compounds are composed only of corner-shared octahedra.

Despite a rapid growth of transition metal oxyhydrides over the previous 5 years,[1−3,10,12−16] these structures have been exclusively limited to perovskite-related compounds having vertex-linked octahedral networks with a M−H−M angle of ∼180°, which may thus limit correlated properties. $ATiO_{3-x}H_x$ (A = alkaline earth elements and Eu),[1−3] $SrCrO_2H$,[13] and $BaScO_2H$[15] adopt a perovskite structure with anion disorder (Figure 1a), while $SrVO_2H$[6] is the anion ordered version (Figure 1b). $LaSrCoO_3H_{0.7}$,[10] $Sr_2VO_{4-x}H_x$,[6,12] and $LaSrMnO_{3.3}H_{0.7}$[14] crystallize in a single-layer (n = 1) Ruddlesden−Popper (RP) layered perovskite structure ($A_{n+1}B_nX_{3n+1}$) with perovskite slabs stacked along $[001]_p$ (Figure 1c). The n = 2 analogues, $Sr_3V_2O_5H_2$[6] and $Sr_3Co_2O_{4.33}H_{0.84}$,[17] are also reported (Figure 1d). $La_2Ti_2O_{6.73}H_{0.02}$[16] with the perovskite slabs along $[110]_p$ is another addition (Figure 1e), although the hydride content is fairly small. It would be therefore interesting to look for transition metal oxyhydrides with face-shared or edge-shared octahedra that enable much smaller M−H−M bridging angles leading to versatile magnetic interactions and thus exhibiting interesting properties.

Herein, we report the high pressure synthesis of $BaVO_{3-x}H_x$ ($0.3 \leq x \leq 0.8$) which adopt a 6H-type hexagonal structure composed of face-shared octahedra as well as corner-shared ones. In $BaVO_{2.7}H_{0.3}$, H^- anions are located exclusively at the face-shared sites, while further H^- incorporation leads to the occupation of both corner- and face-shared sites. This anion order/disorder results in a remarkable difference in their physical properties; we found, from resistivity and nuclear magnetic resonance (NMR) measurements and DFT calculations, that $BaVO_{2.7}H_{0.3}$ is a quasi 2D metal with strong antiferromagnetic (AFM) spin−spin correlations, whereas $BaVO_{2.2}H_{0.8}$ and its cubic polymorph $BaVO_{2.1}H_{0.9}$ (also obtained in this study) show semiconducting behavior, as a result of strong disruption of electron hopping of V t_{2g} electrons via the H 1s ligands.

2. EXPERIMENTAL PROCEDURE

Starting reagents, BaO (99.99%, Aldrich), V_2O_3 (99.99%, Aldrich), and BaH_2 (95%, Aldrich, BaH_2(A)), were used as received for high temperature and high pressure reactions. We later used BaH_2 (BaH_2(B)) which was prepared by heating elemental Ba (99%, Kojundo) under H_2 flow (99.99%, Sumitomo Seika) at 575 °C. These reagents were weighted in a N_2 filled glovebox, according to $y$$BaH_2$ + $(1 - y)$BaO + 1/2 V_2O_3 (y_A = 0.6, y_B = 0, 0.2, 0.3, 0.4, 0.5, 0.6, and 0.8, where y_A and y_B represent fractions of BaH_2(A) and BaH_2(B), respectively), mixed thoroughly in an agate mortar, and sealed in a NaCl capsule inside a pyrophyllite cell with graphic heater. The cell was compressed to a pressure of 3 or 7 GPa using a cubic anvil press, heated at 1000 °C for 30 min, quenched to ambient temperature within 5 min, followed by a slow release of pressure. Polycrystalline samples were recovered from the sample cell as a dense and well-sintered pellet.

We characterized the purity and crystal structures of the samples by powder X-ray diffraction (XRD) measurements using a D8 ADVANCE diffractometer (Bruker AXS) with Cu Kα radiation. High resolution powder synchrotron XRD (SXRD) experiments were performed at room temperature (RT) using a Debye−Scherrer camera with an image plate as a detector, installed at SPring-8 BL02B2 of the Japan Synchrotron Radiation Research Institute (JASRI). Incident beams from a bending magnet were monochromated either to λ = 0.42907 or 0.42073 Å. Sieved powder samples (<32 μm) were loaded into Pyrex capillaries with an i.d. of 0.2 mm. The sealed capillary was rotated during the measurements to reduce the effect of preferred orientation of crystallites. Powder neutron diffraction (ND) data was collected at RT using the high resolution powder diffractometer BT-1 with λ = 1.54060 Å at the NIST Center for Neutron Research (NCNR) and at the IBARAKI Material Design Diffractometer (iMATERIA)[18] at the Japan Proton Accelerator Research Complex (J-PARC). The collected SXRD and ND patterns were analyzed by the Rietveld method using RIETAN-FP program[19] for SXRD and ND (NIST) data and Z-Rietveld program[20,21] for ND (J-PARC) data.

Cation compositions of the obtained materials were measured with energy dispersive X-ray spectroscopy (EDX) using an Oxford X-act detector mounted on a Hitachi S-3400N scanning electron microscope. Hydrogen release behavior upon heating was monitored by a Bruker MS9610 quadrupole mass spectrometer (QMS), where the sample was heated with an Ar flow of 300 mL/min up to 700 °C. Thermogravimetric (TG) measurements were conducted with a Bruker AXS TG-DTA 2000S under flowing oxygen at 300 mL/min up to 700 °C. A platinum pan was used for a sample holder, and Al_2O_3 was used as a reference.

DFT calculations were performed using the projector augmented wave method as implemented in the VASP code.[22,23] An exchange-correlation term was treated with the Perdew−Burke−Ernzerhof functional.[24] We considered all possible structures of the symmetrically independent O/H configurations of a hexagonal unit cell (Figure 2a) with compositions of $Ba_6V_6O_{18-n}H_n$ (where n = 1, 2, ..., 6). Symmetrically nonequivalent configurations (selected using spglib library[25]) amount to 1496, and the number of the models for each composition are given in Table S1. We constructed 1496 input models, and for each model the total energies were minimized until the energy convergences were less than 10^{-5} eV during self-consistent cycles. The atomic positions and lattice constants were relaxed until the residual atomic forces become less than 0.02 eV $Å^{-1}$. Strong correlation effects of 3d orbitals were taken into account within the framework of the GGA+U method.[26] The parameter of effective U potential for V 3d chosen was 3.0 eV.[27,28] Plane-wave cutoff energies were set to 550 eV. Integration in reciprocal space was performed with a 5 × 5 × 2 grid. Furthermore, we analyzed the relationship between formation energies and structural parameters using a linear regression method. A database of the formation energies and the structural

DOI: 10.1021/acs.chemmater.7b04571
Chem. Mater. 2018, 30, 1566−1574

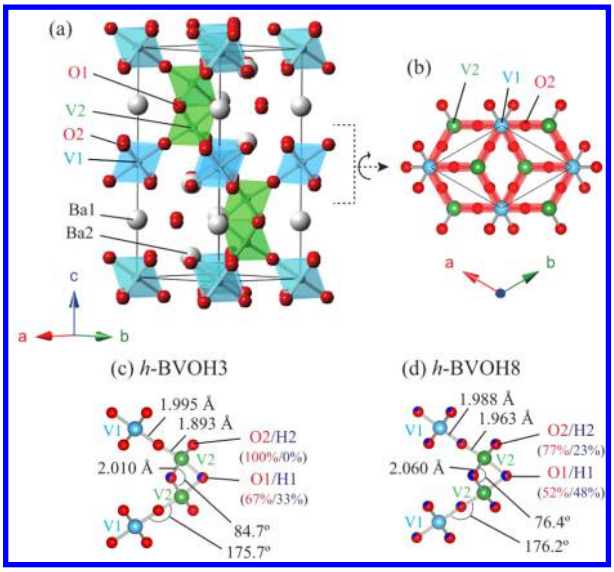

Figure 2. (a) Schematic crystal structure of 6H-type $BaVO_{3-x}H_x$. (b) A 2D network of V1 and V2 connected via O2. Local geometry around vanadium cations for (c) *h*-BVOH3 (x = 0.3) and (d) *h*-BVOH8 (x = 0.8), determined from the neutron refinement. Gray, light blue, green, red, and blue balls represent Ba, V1, V2, O, and H atoms, respectively.

parameters was constructed from the calculations of 1496 independent configurations.

The electrical resistivity down to 2 K was measured by means of a standard four-probe method using a physical property measuring system (Quantum Design, PPMS). Rectangular samples cut from the as-prepared pellets were used. Gold wires were attached to the samples with silver paste. Magnetic susceptibilities were measured on a Quantum Design MPMS-XL SQUID magnetometer, with an applied magnetic field of 0.1 T from 2 to 300 K. We used a conventional spin−echo technique for NMR measurements. ^{51}V NMR spectra (the nuclear spin of I = 7/2 and the nuclear gyromagnetic ratio of $^{51}\gamma/2\pi$ = 11.193 MHz/T) were obtained by sweeping magnetic field in a fixed frequency of 99.1 MHz. The nuclear spin−lattice relaxation rate $1/T_1$ was determined by fitting the time variation of the spin−echo intensity after the saturation of nuclear magnetization to a theoretical function for I = 7/2.

3. RESULTS AND DISCUSSIONS

The laboratory XRD pattern of y_A = 0.6 synthesized at 3 GPa and 1000 °C (where BaH_2(A) was used) was readily indexed using a hexagonal unit cell with a = 5.66 Å and c = 13.77 Å (Figure S1). No peaks associated with impurities or superstructures were found. The obtained pattern resembles with those of a 6H-type perovskite structure consisting of alternate stacking of two face-shared octahedral layers and one corner-shared octahedral layer along the hexagonal c axis (Figure 2a), as found in other transition metal oxides $BaTiO_{3-d}$ (a high temperature form) and $BaCrO_3$.[29,30] A QMS measurement upon heating under an argon gas flow revealed a significant amount of H_2 being released at 250−450 °C (Figure S2). A similar H_2 release behavior has been seen in other oxyhydrides including $ATi(O,H)_3$,[1−3] $BaScO_2H$,[15] and $SrCrO_2H$.[13] A 5H-type $BaVO_{3-d}$ ($0 \leq d \leq 0.2$), which consists of alternate stacking of three face-shared octahedral layers and two corner-shared octahedral layers (Figure S3), was previously prepared in ambient pressure.[31] Under high pressure, only the cubic perovskite (3C) phase of $BaVO_3$ was synthesized (1350 °C at 15 GPa).[32] These facts suggest that the application of pressure and the probable incorporation of hydride anions contribute to stabilize the 6H-type structure.

The SXRD pattern (Figure 3a) contains the hexagonal phase, together with several unknown peaks whose intensities are less

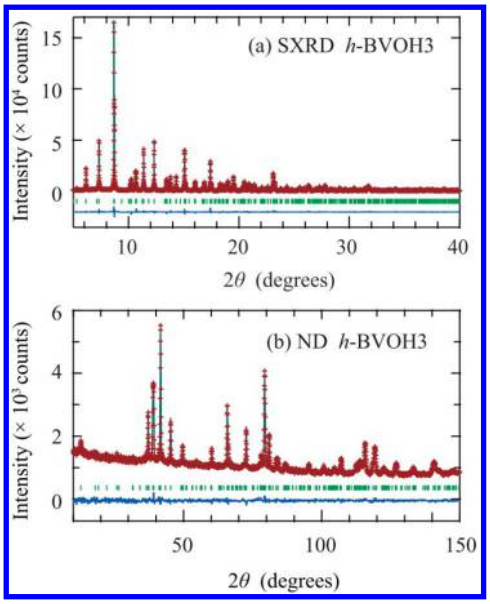

Figure 3. Observed and calculated (a) SXRD (λ = 0.42907 Å) and (b) ND (λ = 1.54060 Å) patterns at RT for $BaVO_{2.7}H_{0.3}$ (*h*-BVOH3). Red overlying crosses and green solid curves represent the observed and the calculated intensities, respectively. The blue solid lines at the bottom indicate the residual curves. Green ticks indicate the peak positions of *h*-BVOH3.

than 1% of the main peak. We refined the experimental profile using the 6H-type structure (space group $P6_3/mmc$), where Ba1 atoms were placed at Wyckoff position 2b (0, 0, 1/4), Ba2 at 4f (1/3, 2/3, z), V1 at 2a (0, 0, 0), V2 at 4f (1/3, 2/3, z), O1 at 6h (x, 2x, 1/4), and O2 at 12k (x, 2x, z). Hydride anions were not considered here. The isotropic displacement parameters B_{iso} of the same elements were set to be equal. The refined occupancy factor of oxygen atom at the O1 site g(O1) was ∼0.7, while no appreciable vacancy was detected at the O2 site (g(O2) = 0.98(1)). Thus, in the following analysis g(O2) was fixed at unity. The refinement was converged, providing agreement indices of R_p = 4.59%, R_{wp} = 6.44%, R_B = 3.14%, R_F = 2.03%, and GoF = 3.02 (Figure 3a and Table 1). The g(O1) of 0.68(1) gives a composition of $BaVO_{2.68(1)}$. TG measurement under oxygen gas flow gave a composition $BaVO_{2.67}$ (Figure 4S), which is well consistent with the SXRD result. EDX analysis confirmed the cation ratio to be Ba/V = 1.

In order to examine the hydrogen content, we performed Rietveld analysis of the constant wavelength ND pattern (Figure 3b). Based on the result of X-ray refinement, we assumed a full oxygen occupation at the O2 site, while a fractional occupancy of hydrogen and oxygen was considered at the O1 site, imposing a constraint of g(O1) + g(H1) = 1. Here, we assumed no vacancy at the anion sites since the vacancy creation could be unfavorable in high pressure condition, as seen in our previous study on (layered) perovskite oxyhydrides.[14,15] The z coordinate and B_{iso} for the vanadium sites were fixed since the neutron scattering length of V is almost zero. The refinement was converged successfully as shown in Figure 3b and Table 1 (R_p = 2.39%, R_{wp} = 3.02%, R_B = 5.63%, R_F = 4.38%, and GoF = 1.01). The refined occupancies of the

DOI: 10.1021/acs.chemmater.7b04571
Chem. Mater. 2018, 30, 1566−1574

Table 1. Crystallographic Parameters for the Hexagonal $BaVO_{2.7}H_{0.3}$ (*h*-BVOH3) from SXRD (Upper) and Constant Wavelength ND (Lower) Refinements[a]

atom	site	g	x	y	z	B_{iso}/Å^2
Ba1	2b	1	0	0	1/4	0.428(8)
						0.13(8)
Ba2	4f	1	1/3	2/3	0.59006(4)	0.428(8)
					0.5913(3)	0.13(8)
V1	2a	1	0	0	0	0.35(2)
V2	4f	1	1/3	2/3	0.1518(1)	0.35(2)
O1	6h	0.68(1)	0.4806(7)	0.9612(7)	1/4	0.55(5)
		0.670(4)	0.4846(6)	0.9692(6)		0.77(3)
O2	12k	1	0.1682(4)	0.3364(4)	0.4178(2)	0.55(5)
		1	0.1671(5)	0.3341(5)	0.4177(1)	0.77(3)
H1	6h					
		0.330(4)	0.4846(6)	0.9692(6)		0.77(3)

[a]Space group: $P6_3/mmc$; $Z = 6$; $a = 5.66726(6)$ Å, and $c = 13.7827(1)$ Å for SXRD and $a = 5.6696(1)$ Å and $c = 13.7891(4)$ Å for ND. $R_p = 4.59\%$, $R_{wp} = 6.44\%$, $R_B = 3.14\%$, $R_F = 2.03\%$, and GoF = 3.02 for SXRD and $R_p = 2.39\%$, $R_{wp} = 3.02\%$, $R_B = 5.63\%$, $R_F = 4.38\%$, and GoF = 1.01 for ND. Values in parentheses indicate one standard deviation.

face-shared anion site are $g(O1)/g(H1) = 0.670(4)/0.330(4)$ corresponding to the 1/3 occupation of H^-. The value of $g(O1)$ agrees well with the one from SXRD. Refining $g(O2)$ gave a value close to 1 ($g(H2) \approx 0$), again in agreement with the result of SXRD. Thus, we conclude that the H^- anion is exclusively located at the face-shared site (Figure 2c) and the composition is $BaVO_{2.670(4)}H_{0.330(4)}$. The compositions obtained from TG ($BaVO_{2.67}$), SXRD ($BaVO_{2.68(1)}$), and ND ($BaVO_{2.670(4)}H_{0.330(4)}$) are very close to each other, suggesting that the anion vacancy, if it exists, is quite small. Accordingly, we set the final composition as $BaVO_{2.7}H_{0.3}$, hereafter denoted as *h*-BVOH3.

During the course of this study, we noticed that BaH_2(A) included a sizable amount of BaO. Thus, we later used a phase pure BaH_2(B) for further preparations. The laboratory XRD pattern of $y_B = 0.8$ synthesized at 3 GPa and 1000 °C using BaH_2(B) is similar to that of *h*-BVOH3 (Figure S5), but it has a larger unit cell of $a = 5.70$ Å and $c = 13.81$ Å, indicating further incorporation of H^-. A cubic phase was also found, assigned to a perovskite $BaVO_{3-x}H_x$ ($x \approx 1$; $a \approx 4.01$ Å), as will be discussed later. The QMS of this specimen showed a release of H_2 at around 250−650 °C (Figure S6), with the ion current at the peak roughly twice of that of *h*-BVOH3, supporting a greater H^- content. This is further supported by the TG measurement which gave a composition of $BaVO_{2.21}$ (Figure S7). EDX analysis confirmed the cation ratio of Ba/V = 1:1. The Rietveld analyses of SXRD and ND data (Figure 4) were performed using the 6H-type structure, with the cubic perovskite $BaVO_{3-x}H_x$ added as a secondary phase, and the results are summarized in Table 2. As opposed to *h*-BVOH3, the ND analysis probed H^- both at the face- and corner-shared sites (Figure 2d), with the anion occupancies of $g(O1)/g(H1) = 0.524(2)/0.476(2)$ and $g(O2)/g(H2) = 0.766(4)/0.234(4)$. The SXRD analysis is consistent with this observation: $g(O1) = 0.57(1)$ and $g(O2) = 0.90(1)$. The compositions obtained from ND ($BaVO_{2.056(6)}H_{0.944(6)}$), SXRD ($BaVO_{2.37(3)}$), and TG ($BaVO_{2.21}$) are scattered to some extent possibly due to the presence of the cubic $BaVO_{3-x}H_x$ impurity (12 wt %). In any event, the hydride amount is much greater than that in *h*-BVOH3. We will use an averaged composition of $BaVO_{2.2}H_{0.8}$ (*h*-BVOH8). Note that its hydride content is somewhat smaller than the nominal composition, implying that excess hydrogen (or H_2 pressure) is necessary to stabilize the oxyhydride phase,

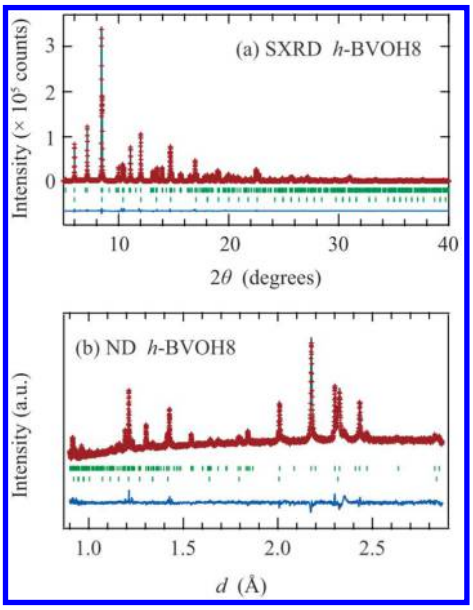

Figure 4. Observed and calculated (a) SXRD ($\lambda = 0.42073$ Å) and (b) time-of-flight ND patterns at RT for $BaVO_{2.2}H_{0.8}$ (*h*-BVOH8). Upper and lower green ticks indicate the peak positions of *h*-BVOH8 and the cubic perovskite $BaVO_{3-x}H_x$ (a mass fraction of 12%), respectively.

a tendency that has also been observed in other oxyhydrides.[12,14]

When y_B was varied (y_B = 0, 0.2, 0.3, 0.4, 0.5, 0.6, and 0.8), we also obtained the 6H-type structure (Figure S5), except for $y_B = 0$ which resulted in $Ba_3V_2O_8$[33] and unknown impurity phases. A systematic evolution of lattice parameters is only seen for $0.2 \leq y_B \leq 0.5$ (Figure 5). A gradual increase of the cell parameters from $y_B = 0.2$ to 0.5 indicates that the hydride content increases with y_B. The $y_B = 0.2$ sample has lattice parameters close to *h*-BVOH3 ($y_A = 0.6$), suggesting that *h*-BVOH3 ($x \approx 0.3$) roughly gives a lower limit of the hydride content in $BaVO_{1-x}H_x$ for the 6H-type phase. Likewise, the saturation of cell parameters above $y_B = 0.5$ suggests an upper solubility limit of $x \approx 0.8$ (*h*-BVOH8).

We have already shown that the sample of *h*-BVOH8 contains a small amount of cubic perovskite (3C) phase with $a = 4.00$ Å. This cubic phase can be isolated by elevating pressure to 7 GPa ($y_B = 0.6$ at 1000 °C), as shown in Figure S8. $BaVO_3$

DOI: 10.1021/acs.chemmater.7b04571
Chem. Mater. 2018, 30, 1566−1574

Table 2. Crystallographic Parameters for the Hexagonal $BaVO_{2.2}H_{0.8}$ (*h*-BVOH8) from SXRD (Upper) and Time-of-Flight ND (Lower) Refinements[a]

atom	site	*g*	*x*	*y*	*z*	B_{iso}/Å^2
Ba1	2b	1	0	0	1/4	0.55(1)
						0.35(6)
Ba2	4f	1	1/3	2/3	0.58692(6)	0.55(1)
					0.5886(3)	0.35(6)
V1	2a	1	0	0	0	0.46(2)
V2	4f	1	1/3	2/3	0.1577(1)	0.46(2)
O1	6h	0.57(1)	0.483(1)	0.966(1)	1/4	1.2(1)
		0.524(2)	0.497(3)	0.994(3)		0.10(4)
O2	12k	0.90(1)	0.1677(7)	0.3353(7)	0.4160(4)	1.2(1)
		0.766(4)	0.1641(5)	0.3282(5)	0.4167(2)	0.10(4)
H1	6h					
		0.476(2)	0.497(3)	0.994(3)		0.10(4)
H2	12k					
		0.234(4)	0.1641(5)	0.3282(5)	0.4167(2)	0.10(4)

[a]Space group: $P6_3/mmc$; $Z = 6$; $a = 5.70649(5)$ Å and $c = 13.8055(1)$ Å for SXRD and $a = 5.70620(3)$ Å and $c = 13.8067(2)$ Å for ND. $R_p = 4.28\%$, $R_{wp} = 7.27\%$, $R_B = 2.90\%$, $R_F = 1.62\%$, and GoF = 5.32 for SXRD and $R_p = 1.83\%$, $R_{wp} = 2.28\%$, $R_B = 6.86\%$, $R_F = 9.01\%$, and GoF = 1.36 for ND.

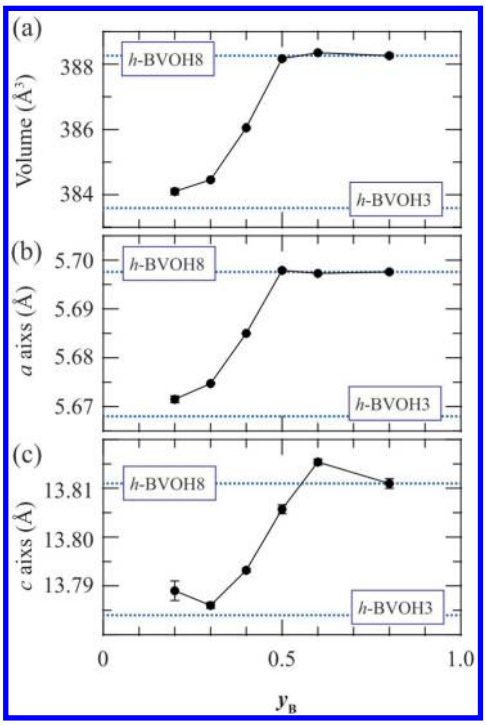

Figure 5. Lattice parameters and volume of the 6H phase of $BaV(O,H)_3$ as a function of y_B, where the samples were prepared in a starting mixture of $y_BBaH_2 + (1 - y_B)BaO + 1/2\ V_2O_3$. Upper and lower dashed lines respectively represent the values for *h*-BVOH8 and *h*-BVOH3. *h*-BVOH3 was synthesized using BaH_2(a).

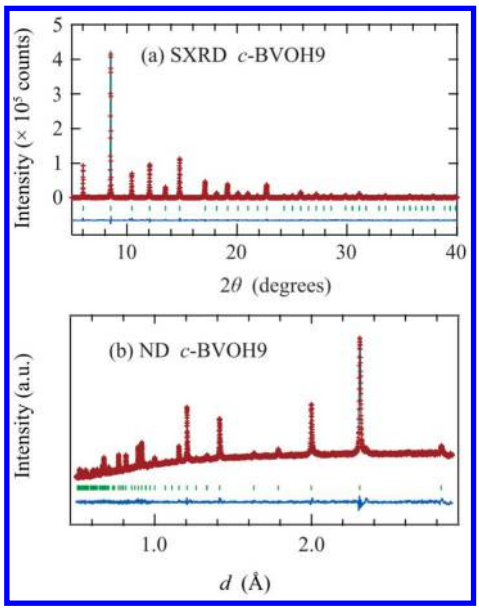

Figure 6. Observed and calculated (a) SXRD ($\lambda = 0.42073$ Å) and (b) time-of-flight ND patterns at RT for the cubic $BaVO_{2.1}H_{0.9}$ (*c*-BVOH9), adopting the ideal perovskite structure (Pm-$3m$), with $a = 3.99830(3)$ Å, $g(O) = 0.728(4)$, $B_{iso}(Ba) = 0.446(6)$, $B_{iso}(V) = 0.55(1)$, and $B_{iso}(O) = 0.74(5)$ for SXRD and $a = 3.99901(2)$ Å, $g(O)/g(H) = 0.684(2)/0.316(2)$, $B_{iso}(Ba) = 0.20(3)$, $B_{iso}(V) = 0.55$, and $B_{iso}(O/H) = 0.28(2)$ for ND. Agreement indices are $R_p = 4.99\%$, $R_{wp} = 8.11\%$, $R_B = 2.25\%$, $R_F = 1.31\%$, and GoF = 4.07 for SXRD and $R_p = 2.22\%$, $R_{wp} = 2.64\%$, $R_B = 5.67\%$, $R_F = 9.92\%$, and GoF = 1.27 for ND.

has been known to exist at much higher pressures of around 15 GPa,[32] with a shorter *a* axis of 3.94 Å, indicating that our sample is more reduced in terms of the titanium valence. In fact, TG measurement yielded $BaVO_{2.12}$ (Figure S9), and QMS signified a substantial amount of H_2 upon heating (Figure S10). Thus, we conducted Rietveld refinement of SXRD and ND (Figure 6) using the ideal perovskite structure ($Pm\bar{3}m$) of $BaVO_{3-x}H_x$ (Figure 1a), which yielded $BaVO_{2.052(6)}H_{0.948(6)}$. We will hereafter use *c*-BVOH9 ($BaVO_{2.1}H_{0.9}$) unless indicated otherwise. The bond valence sum (BVS) value for V is +2.7, which is similar to that of *h*-BVOH8 as shown later. The calculated density of *c*-BVOH9, 5.77 g/cm^3, is higher than 5.69 g/cm^3 for the almost isocompositional *h*-BVOH8, justifying the formation (and stabilization) of the former under higher pressure. Similar hexagonal-to-cubic perovskite transitions by pressurization were reported previously in oxides.[34,35] We would like to point out that $SrVO_2H$ (Figure 1b) forms the infinite-layer structure. For perhaps, the ionic size of Ba is too large to adopt the infinite-layer structure. Similarly, the infinite-layer oxide $SrFeO_2$ undergoes a transition upon Ba-for-Sr substitution,[36] leading to a structure that is analogous to the Brownmillerite structure.[37]

DOI: 10.1021/acs.chemmater.7b04571
Chem. Mater. 2018, 30, 1566−1574

The local structures of *h*-BVOH3 and *h*-BVOH8 are presented in Figure 2c,d. V−O (and V−H) bond lengths of 1.893−2.060 Å are comparable with other oxides with VO_6 octahedra.[31,32,38] The V−H bond is similar to that of $Sr_2VO_{4-x}H_x$ ($x \leq 0.7$)[12] but is longer than 1.83 Å for $Sr_{n+1}V_nO_{2n+1}H_n$ (n = 1, 2, ∞), which is not surprising given the complete H/O order and the resultant compression of the hydride anion.[6,9] We calculated the BVS values for V1 and V2 in *h*-BVOH3/*h*-BVOH8 using literature parameters[39,40] and obtained +3.4/+2.8 and +3.6/+2.6, respectively, in reasonable agreement with those expected from the hydride compositions ($V^{3.7+}/V^{3.2+}$). The bridging angles ∠V1−O2−V2 for corner-shared octahedra are slightly smaller than 180°: 175.7° in *h*-BVOH3 and 176.2° in *h*-BVOH8. The ∠V2−O1−V2 angle for face-shared octahedra in *h*-BVOH3 is 84.7°, which is larger than 76.4° for *h*-BVOH8. This change results from the "asymmetric" coordination environment around V2 in *h*-BVOH3. Namely, the site-selective hydride occupation at O1 leads to a more pronounced V2 displacement toward the O2 triangular plane.

In *h*-BVOH3, all of the H^- anions occupy the face-shared site. Similarly, oxygen vacancy has been created selectively at the face-shared site (vs corner-shared site) in related structures such as 6H-$BaTiO_{2.85}$,[29] 4H-$BaMnO_{3-\delta}$ ($\delta \leq 0.35$),[41] and 6H-$BaFeO_{2.91}$.[42] Such selective creation of vacancy in these oxides may be understood in terms of a weaker bonding for the face-shared M−O−M with ∠M−O−M ≈ 80° than for the corner-shared one with ∠M−O−M ≈ 180°. We note that in ref 41 the authors referred to the Ba−O bond length as a key parameter for the preference. However, this scenario cannot explain what happened to our case (*h*-BVOH3) since all of the Ba−O bond lengths are fairly close (2.835−2.898 Å). Also note that a 5H-type $BaMO_{2.8}$ phase (M = V, Cr, and Fe) has oxygen vacancy at the corner-shared site, as a result of an oxygen vacancy order giving double layers of MO_4 tetrahedra (Figure S3).[31,43,44] These examples imply that, like anion-deficient oxides, hydride positioning in hexagonal perovskite-based oxyhydrides can be tailored in various ways.

In order to obtain further insight into the location of hydride anion as a function of hydride content, we calculated energies of all possible independent 1496 configurations of $Ba_6V_6O_{18-n}H_n$ (n= 1, 2, ..., 6; Table S1) and obtained the most stable configurations for each n as shown in Figure 7 and Table 3. For n = 1 (corresponding approximately to $BaVO_{2.83}H_{0.17}$), there are two independent configurations, and the configuration with H^- at the face-shared (6*h*) site (Figure 7a) is more stable than the one at the corner-shared site by 170 meV. For n = 2 ($BaVO_{2.67}H_{0.33}$), we compared 14 independent models, and the most stable configuration (Figure 7b) is where H^- anions are positioned only at the 6h site, in excellent agreement with the structure found in *h*-BVOH3 ($BaVO_{2.670(4)}H_{0.330(4)}$). The second most stable one also has H^- anions only at the 6h site, while H^- anions are found both at the 6h and 12k sites for the third and fourth ones, whose energies are greater by 305 and 492 meV relative to the most stable configuration (Figure S11 and Table 2).

One can see from Figure 7c−f that, with further increasing n, additional H^- anions are also occupied at the corner-shared (12k) site, as experimentally observed for *h*-BVOH8. The most stable configuration of the "terminal" composition $Ba_6V_6O_{12}H_6$ (n = 6, x = 1) has 2 and 4 hydride anions respectively at 6h and 12k sites, meaning the loss of site preference, which is inconsistent with *h*-BVOH8 that retains the partial face-shared preference (g(H1) = 0.476 and g(H2) = 0.234). Nevertheless,

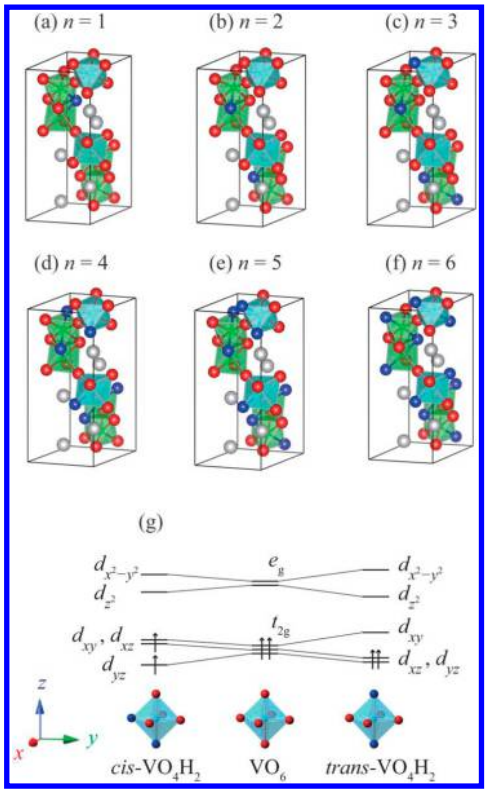

Figure 7. (a−f) Most stable structures in the 6H-type system for $Ba_6V_6O_{18-n}H_n$ (n = 1, 2, ..., 6) obtained by the DFT calculations. Gray, light blue, green, red, and blue balls represent Ba, V1, V2, O, and H atoms, respectively. (g) Crystal-field splitting of V 3d orbitals in cis- and trans-$V^{III}O_4H_2$ octahedron, showing the trans preference for $1 < n' \leq 2$ (n': d electron count).

Table 3. Numbers of H^- in Face-Shared (6h) or Corner-Shared (12k) sites and Those of cis- or trans-Coordinate Octahedra in the Most Stable Structures of $Ba_6V_6O_{18-n}H_n$ in Figure 7

n in $Ba_6V_6O_{18-n}H_n$	1	2	3	4	5	6
no. of H^- at 6h	1	2	2	2	2	2
no. of H^- at 12k	0	0	1	2	3	4
no. of *cis*-VO_4H_2	0	0	0	0	1	0
no. of *trans*-VO_4H_2	0	0	1	2	3	6

our DFT calculations for $n \geq 3$ (Table 3) shows an interesting implication on the local structure of the VO_4H_2 octahedra, that is, the preference of the trans configuration (vs the cis configuration). For n = 3 ($BaVO_{2.5}H_{0.5}$), the most stable configuration has one trans-coordinate octahedron in the unit cell (Figure 7c), while the second and third ones have one cis-coordinate octahedron with energies higher by 137 and 220 meV (Figure S12 and Table S3). Similar trends are also observed for n = 4−6.

In order to further examine trans/cis coordination preference (impossible to probe by conventional Rietveld refinements), we carried out a regression analysis of the energy calculations, where all 1496 configurations were statistically taken into account (see the Supporting Information). Figure S14 shows that the coefficients for trans and cis configurations of VO_4H_2 octahedra take large negative and positive values, respectively, meaning that the former configuration is favorable. Note that the preference at the face-shared site (vs corner) is also seen

DOI: 10.1021/acs.chemmater.7b04571
Chem. Mater. 2018, 30, 1566−1574

from its large negative coefficient. The theoretically suggested trans preference in VO_4H_2 octahedra for $3 \leq n \leq 6$ can be rationalized by the crystal field splitting of V 3d orbitals with d electron count n' of 1.5−2, as shown in Figure 7g. The trans preference of electronic origin is more explicitly seen in $SrVO_2H$ (d^2) with the complete anion order (Figure 1b).[6] This study, in contrast, suggests the same trend even in the case where n' is noninteger ($1 < n' \leq 2$).

Now we have three oxyhydrides of $BaVO_{3-x}H_x$, with different structural types (6H vs 3C), different hydride contents (x = 0.3 vs 0.8 for 6H), and anion order/disorder. These features may bring about certain differences in physical properties. Indeed, electrical resistivity experiments (Figure 8a) have revealed that the physical property of *h*-BVOH3 differs significantly from those of *h*-BVOH8 and *c*-BVOH9. The electrical resistivity of the sintered pellet of *h*-BVOH3 shows a metallic behavior, in marked contrast to the other two compounds with higher electrical resistivities and semiconducting temperature dependences. Arrhenius fitting above 200 K gave activation energies of 0.05 and 0.12 eV for *h*-BVOH8 and *c*-BVOH9 (Figure S15). The resistivity of *h*-BVOH3 up to 50 K was fitted by $\rho = \rho_0 + AT^{\alpha}$ (inset of Figure 8a), where ρ_0, A, and α represent the residual resistivity, the temperature coefficient, and the exponent. Remarkably, the exponent α is estimated as 0.75, which is smaller than what is expected from a Fermi liquid (α = 2), implying an anomalous metallic state.

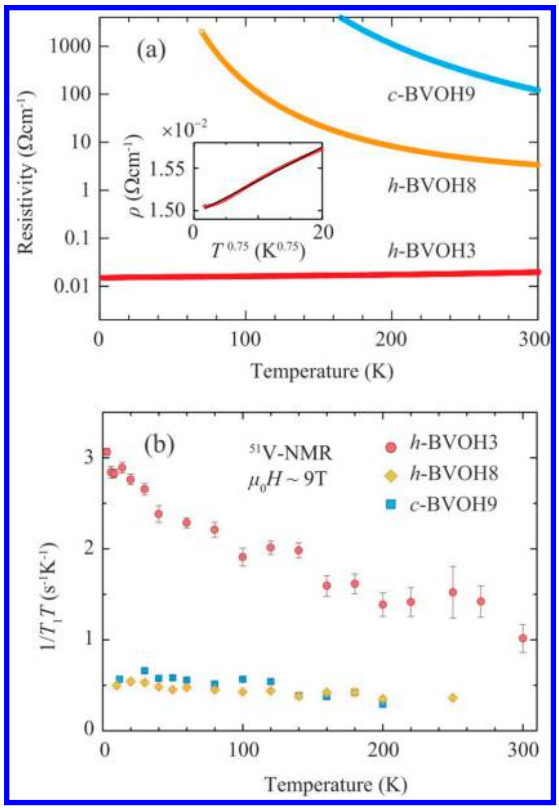

Figure 8. Temperature dependence of (a) electric resistivity and (b) spin−lattice relaxation rate $1/T_1T$ for *h*-BVOH3, *h*-BVOH8, and *c*-BVOH9. The inset in (a) magnifies the resistivity for *h*-BVOH3 below 50 K, fitted to $\rho = \rho_0 + AT^{\alpha}$ (α = 0.75). NMR spectra signified no magnetic transition down to 1.5 K for *h*-BVOH3 and to 10 K for *h*-BVOH8 and *c*-BVOH9 (Figure S17).

The magnetic susceptibility of *h*-BVOH3 (Figure S16) is almost temperature independent, a behavior typical for a paramagnetic metal, although it slightly increases at low temperatures. On the other hand, *h*-BVOH8 exhibits more pronounced temperature dependence, indicating the localized nature of spins. A Curie−Weiss fitting above 200 K gives a Curie constant of C = 0.16 emu/K mol, giving the effective moment of μ_{eff} = 1.1 μ_B. This value is much smaller than ∼2.8 μ_B assuming completely localized d electrons ($V^{3.1+}$; $d^{1.9}$). This suggests that the d electrons are localized but not completely in accordance with the $\rho-T$ data, although clarifying in-depth transport property is difficult given the use of powder specimen. The magnetic susceptibility of *c*-BVOH9 is qualitatively similar to *h*-BVOH8, with C = 0.20 emu/K mol. Note that a small anomaly in susceptibilities of *h*-BVOH8 and *c*-BVOH9 at 21 K that come from a tiny magnetic impurity as NMR spectra (Figure S17) did not show any change across this temperature.

What is the origin of the remarkable difference in the transport property between *h*-BVOH3 and *h*-BVOH8? To answer this, let us consider for simplicity a hypothetical 6H-type oxide $BaVO_3$ though the electron doping rate is smaller. In general, the d electron hopping interaction in oxides is mostly mediated by the O 2p orbital and hence is sensitive to the oxygen bridging angle. Clearly, the orbital overlap by indirect transfer between V t_{2g} orbitals through the O 2p orbital is much greater for the corner-shared octahedra with a nearly linear V1−O2−V2 bond than for the face-shared ones with a heavily bent V2−O1−V2 bond. Thus, the transport property of this hypothetical oxide should be anisotropic, with a superior in-plane conductivity expected within the V1−O2−V2 network (see Figure 2b). In fact, the calculated band structure of 6H-$BaVO_3$ (d^1) has a quasi 2D feature (Figure S18) and in-plane conductivity at 300 K is 1 order of magnitude higher than the out-of-plane conductivity (Figure S19), although we admit that the magnitude of the anisotropy may vary with the electron doping rate.

When the O1 site is partially replaced by hydride anion (as occurred in *h*-BVOH3), the d electron hopping between face-shared octahedra (i.e., along *c*) will be significantly interrupted by a nearly orthogonal arrangement between H 1s and V t_{2g} orbitals and by chemical disorder along this axis, whereas the in-plane conduction path remains intact, and hence conduction electrons may be effectively confined within the V1−O2−V2 slab. In addition, the electrical conductivity in "6H-$BaVO_3$" with electron doping rate of 0.3/vanadium is highly anisotropic (Figure 19S), implying a quasi 2D metallic state in *h*-BVOH3. In contrast, the hydride anions in *h*-BVOH8 are also occupied at the O2 site, and this may interrupt the in-plane conductivity, leading to a semiconducting behavior (Figure 8a). We also found that the degree of anisotropy in 6H-$BaVO_3$ is reduced when the electron doping rate is increased (see the result for 0.8/vanadium in Figure 19S). It was deduced that the semiconducting behavior of *c*-BVOH9 is also a reflection of the interrupted electron hopping by the hydride ligand, along with chemical disorder.

To gain microscopic information on the electronic states of these oxyhydrides, we performed ^{51}V NMR experiments and again observed a distinct feature in *h*-BVOH3. As shown in Figure 8b, $1/T_1T$ for *h*-BVOH3 increases with lowering temperature, which manifests strong AFM fluctuations. Such strong AFM fluctuations are mostly likely resulting from the enhanced two dimensionality since a similar behavior has been observed, e.g., in the parent compounds of iron-based superconductors such as $BaFe_2(As,P)_2$.[45,46] It is thus possible that the anomalous metallic state observed in the electrical

DOI: 10.1021/acs.chemmater.7b04571
Chem. Mater. 2018, 30, 1566−1574

resistivity measurement is linked to the AFM fluctuations. In fact, $\alpha = 0.75$ in *h*-BVOH3 is close to the expected value of $\alpha = 1$ for a system with 2D AFM fluctuations.[47] $BaFe_2(As_{0.7}P_{0.3})_2$ has a similar value.[48] In contrast, the $1/T_1T$ curves for *h*-BVOH8 and *c*-BVOH9 are almost temperature independent. Together with resistivity and susceptibility data, we consider that the AFM fluctuations of *h*-BVOH8 and *c*-BVOH9 are much weaker.

4. CONCLUSION

Using high pressure synthesis at 3 GPa, we synthesized a novel oxyhydride $BaVO_{3-x}H_x$ ($0.3 \leq x \leq 0.8$) with a hexagonal 6H-structure having both face- and corner-shared octahedra. Structural characterizations and DFT calculations have revealed that, at $x = 0.3$ (*h*-BVOH3), H^- anions are located exclusively at the face-shared sites. It is likely that this selective hydride occupation makes its transport properties quasi 2D and is responsible for its anomalous metallic behavior with strong AFM fluctuations. On the other hand, $x = 0.8$ (*h*-BVOH8) contains H^- anions at both face- and corner-shared sites with a partial preference for the former. Additionally, a trans preference in the VO_4H_2 octahedron is theoretically suggested in a H^- rich region. *h*-BVOH8 and its cubic polymorph stabilized at 7 GPa exhibit a semiconducting behavior with weak spin−spin correlations. In oxides, various types of stacking patterns of corner- and face-shared octahedral layers are known such as 2H, 4H, and 9R structures (Figure 3S).[41,43,49−52] Thus, it is expected that a large family of hexagonal oxyhydrides will be prepared in the future, and they might exhibit novel physical properties that might be linked to the stacking sequence as well as the selective hydride distributions.

■ ASSOCIATED CONTENT

Supporting Information

The Supporting Information is available free of charge on the ACS Publications website at DOI: 10.1021/acs.chemmater.7b04571.

Supporting graphics (Figures S1−S19) and tables (Tables S1−S4); regression analysis of energy calculations; electrical conductivity calculation; and supporting references. (PDF)

■ AUTHOR INFORMATION

Corresponding Author

*E-mail: kage@scl.kyoto-u.ac.jp.

ORCID

Takafumi Yamamoto: 0000-0002-7960-1014
Kotaro Fujii: 0000-0003-3309-9118
Masatomo Yashima: 0000-0001-5406-9183
Hiroshi Kageyama: 0000-0002-3911-9864

Notes

The authors declare no competing financial interest.

■ ACKNOWLEDGMENTS

This work was supported by JSPS KAKENHI Grant Nos. JP16H06438, JP16H06439, JP16H06440, JP16H06033, 16K21724, and JP17H05481. This work was also supported by CREST (JPMJCR1421). This work was partially supported by MI2I project of JST. The SXRD experiments were performed at the BL02B2 of SPring-8 with the approval of JASRI (2014B1360 and 2015B1111). The ND experiment was performed at J-PARC (2014B0114 and 2015A0249) and the NIST Center for Neutron Research.

■ REFERENCES

(1) Kobayashi, Y.; Hernandez, O. J.; Sakaguchi, T.; Yajima, T.; Roisnel, T.; Tsujimoto, Y.; Morita, M.; Noda, Y.; Mogami, Y.; Kitada, A.; Ohkura, M.; Hosokawa, S.; Li, Z.; Hayashi, K.; Kusano, Y.; Kim, J. e.; Tsuji, N.; Fujiwara, A.; Matsushita, Y.; Yoshimura, K.; Takegoshi, K.; Inoue, M.; Takano, M.; Kageyama, H. An oxyhydride of $BaTiO_3$ exhibiting hydride exchange and electronic conductivity. *Nat. Mater.* **2012**, *11*, 507−511.

(2) Sakaguchi, T.; Kobayashi, Y.; Yajima, T.; Ohkura, M.; Tassel, C.; Takeiri, F.; Mitsuoka, S.; Ohkubo, H.; Yamamoto, T.; Kim, J. E.; Tsuji, N.; Fujihara, A.; Matsushita, Y.; Hester, J.; Avdeev, M.; Ohoyama, K.; Kageyama, K. Oxyhydrides of (Ca, Sr, Ba)TiO_3 Perovskite Solid Solutions. *Inorg. Chem.* **2012**, *51*, 11371−11376.

(3) Yamamoto, T.; Yoshii, R.; Bouilly, G.; Kobayashi, Y.; Fujita, K.; Kususe, Y.; Matsushita, Y.; Tanaka, K.; Kageyama, H. An Antiferro-to-Ferromagnetic Transition in $EuTiO_{3-x}H_x$ Induced by Hydride Substitution. *Inorg. Chem.* **2015**, *54*, 1501−1507.

(4) Yajima, T.; Takeiri, F.; Aidzu, K.; Akamatsu, H.; Fujita, K.; Yoshimune, W.; Ohkura, M.; Lei, S.; Gopalan, V.; Tanaka, K.; Brown, C. M.; Green, M. A.; Yamamoto, T.; Kobayashi, Y.; Kageyama, H. A labile hydride strategy for the synthesis of heavily nitridized $BaTiO_3$. *Nat. Chem.* **2015**, *7*, 1017−1023.

(5) Masuda, N.; Kobayashi, Y.; Hernandez, O.; Bataille, T.; Paofai, S.; Suzuki, H.; Ritter, C.; Ichijo, N.; Noda, Y.; Takegoshi, K.; Tassel, C.; Yamamoto, T.; Kageyama, H. Hydride in $BaTiO_{2.5}H_{0.5}$: A Labile Ligand in Solid State Chemistry. *J. Am. Chem. Soc.* **2015**, *137*, 15315−15321.

(6) Denis Romero, F.; Leach, A.; Möller, J. S.; Foronda, F.; Blundell, S. J.; Hayward, M. A. Strontium Vanadium Oxide−Hydrides:"Square-Planar" Two-Electron Phases. *Angew. Chem., Int. Ed.* **2014**, *53*, 7556−7559.

(7) Wei, Y.; Gui, H.; Li, X.; Zhao, Z.; Zhao, Y.; Xie, W. The effect of hydrogen ordering on the electronic and magnetic properties of the strontium vanadium oxyhydride. *J. Phys.: Condens. Matter* **2015**, *27*, 206001.

(8) Liu, K.; Hou, Y.; Gong, X.; Xiang, H. Orbital Delocalization and Enhancement of Magnetic Interactions in Perovskite Oxyhydrides. *Sci. Rep.* **2016**, *6*, 19653.

(9) Yamamoto, T.; Zeng, D.; Kawakami, T.; Arcisauskaite, V.; Yata, K.; Patino, M.; Izumo, N.; McGrady, J.; Kageyama, H.; Hayward, M. A. The role of π-blocking hydride ligands in a pressure-induced insulator to metal phase transition in $SrVO_2H$. *Nat. Commun.* **2017**, *8*, 1217.

(10) Hayward, M. A.; Cussen, E.; Claridge, J.; Bieringer, M.; Rosseinsky, M.; Kiely, C.; Blundell, S.; Marshall, I.; Pratt, F. The hydride anion in an extended transition metal oxide array: $LaSrCoO_3H_{0.7}$. *Science* **2002**, *295*, 1882−1884.

(11) Bridges, C. A.; Darling, G. R.; Hayward, M. A.; Rosseinsky, M. J. Electronic structure, magnetic ordering, and formation pathway of the transition metal oxide hydride $LaSrCoO_3H_{0.7}$. *J. Am. Chem. Soc.* **2005**, *127*, 5996−6011.

(12) Bang, J.; Matsuishi, S.; Hiraka, H.; Fujisaki, F.; Otomo, T.; Maki, S.; Yamaura, J.; Kumai, R.; Murakami, Y.; Hosono, H. Hydrogen ordering and new polymorph of layered perovskite oxyhydrides: $Sr_2VO_{4-x}H_x$. *J. Am. Chem. Soc.* **2014**, *136*, 7221−7224.

(13) Tassel, C.; Goto, Y.; Kuno, Y.; Hester, J.; Green, M.; Kobayashi, Y.; Kageyama, H. Direct Synthesis of Chromium Perovskite Oxyhydride with a High Magnetic-Transition Temperature. *Angew. Chem., Int. Ed.* **2014**, *53*, 10377−10380.

(14) Tassel, C.; Goto, Y.; Watabe, D.; Tang, Y.; Lu, H.; Kuno, Y.; Takeiri, F.; Yamamoto, T.; Brown, C. M.; Hester, J.; Kobayashi, Y.; Kageyama, H. High-Pressure Synthesis of Manganese Oxyhydride with Partial Anion Order. *Angew. Chem., Int. Ed.* **2016**, *55*, 9667−9670.

(15) Goto, Y.; Tassel, C.; Noda, Y.; Hernandez, O.; Pickard, C. J.; Green, M. A.; Sakaebe, H.; Taguchi, N.; Uchimoto, Y.; Kobayashi, Y.;

DOI: 10.1021/acs.chemmater.7b04571
Chem. Mater. 2018, 30, 1566−1574

Kageyama, H. Pressure-Stabilized Cubic Perovskite Oxyhydride $BaScO_2H$. *Inorg. Chem.* **2017**, *56*, 4840−4845.
(16) Pussacq, T.; Kabbour, H.; Colis, S.; Vezin, H.; Saitzek, S.; Gardoll, O.; Tassel, C.; Kageyama, H.; Laberty Robert, C.; Mentré, O. Reduction of $Ln_2Ti_2O_7$ Layered Perovskites: A Survey of the Anionic Lattice, Electronic Features, and Potentials. *Chem. Mater.* **2017**, *29*, 1047−1057.
(17) Helps, R. M.; Rees, N. H.; Hayward, M. A. $Sr_3Co_2O_{4.33}H_{0.84}$: An Extended Transition Metal Oxide-Hydride. *Inorg. Chem.* **2010**, *49*, 11062−11068.
(18) Ishigaki, T.; Hoshikawa, A.; Yonemura, M.; Morishima, T.; Kamiyama, T.; Oishi, R.; Aizawa, K.; Sakuma, T.; Tomota, Y.; Arai, M. IBARAKI materials design diffractometer (iMATERIA)−Versatile neutron diffractometer at J-PARC. *Nucl. Instrum. Methods Phys. Res., Sect. A* **2009**, *600*, 189−191.
(19) Izumi, F.; Momma, K. Three-dimensional visualization in powder diffraction. *Solid State Phenom.* **2007**, *130*, 15−20.
(20) Oishi, R.; Yonemura, M.; Nishimaki, Y.; Torii, S.; Hoshikawa, A.; Ishigaki, T.; Morishima, T.; Mori, K.; Kamiyama, T. Rietveld analysis software for J-PARC. *Nucl. Instrum. Methods Phys. Res., Sect. A* **2009**, *600*, 94−96.
(21) Oishi-Tomiyasu, R.; Yonemura, M.; Morishima, T.; Hoshikawa, A.; Torii, S.; Ishigaki, T.; Kamiyama, T. Application of matrix decomposition algorithms for singular matrices to the Pawley method in Z-Rietveld. *J. Appl. Crystallogr.* **2012**, *45*, 299−308.
(22) Kresse, G.; Hafner, J. Ab initio molecular dynamics for liquid metals. *Phys. Rev. B: Condens. Matter Mater. Phys.* **1993**, *47*, 558−561.
(23) Kresse, G.; Furthmüller, J. Efficient iterative schemes for ab initio total-energy calculations using a plane-wave basis set. *Phys. Rev. B: Condens. Matter Mater. Phys.* **1996**, *54*, 11169−11186.
(24) Perdew, J. P.; Burke, K.; Ernzerhof, M. Generalized gradient approximation made simple. *Phys. Rev. Lett.* **1996**, *77*, 3865−3868.
(25) Togo, A. SPGLIB: A C library for finding and handling crystal symmetries; https://atztogo.github.io/spglib/; accessed 06/12/2017.
(26) Dudarev, S.; Botton, G.; Savrasov, S.; Humphreys, C.; Sutton, A. Electron-energy-loss spectra and the structural stability of nickel oxide: An LSDA U study. *Phys. Rev. B: Condens. Matter Mater. Phys.* **1998**, *57*, 1505−1509.
(27) Wang, L.; Maxisch, T.; Ceder, G. Oxidation energies of transition metal oxides within the GGA U framework. *Phys. Rev. B: Condens. Matter Mater. Phys.* **2006**, *73*, 195107.
(28) Jain, A.; Hautier, G.; Ong, S. P.; Moore, C. J.; Fischer, C. C.; Persson, K. A.; Ceder, G. Formation enthalpies by mixing GGA and GGA U calculations. *Phys. Rev. B: Condens. Matter Mater. Phys.* **2011**, *84*, 045115.
(29) Sinclair, D.; Skakle, J. S.; Morrison, F.; Smith, R.; Beales, T. Structure and electrical properties of oxygen-deficient hexagonal $BaTiO_3$. *J. Mater. Chem.* **1999**, *9*, 1327−1331.
(30) Arevalo-Lopez, A. M.; Reeves, S. J.; Attfield, J. P. Ferrimagnetism in the High Pressure 6H-Perovskite $BaCrO_3$. *Z. Anorg. Allg. Chem.* **2014**, *640*, 2727−2729.
(31) Liu, G.; Greedan, J. E. Syntheses, structures, and characterization of 5-layer $BaVO_{3-x}$ (x = 0.2, 0.1, 0.0). *J. Solid State Chem.* **1994**, *110*, 274−289.
(32) Nishimura, K.; Yamada, I.; Oka, K.; Shimakawa, Y.; Azuma, M. High-pressure synthesis of $BaVO_3$: A new cubic perovskite. *J. Phys. Chem. Solids* **2014**, *75*, 710−712.
(33) Parhi, P.; Manivannan, V.; Kohli, S.; Mccurdy, P. Synthesis and characterization of $M_3V_2O_8$ (M= Ca, Sr and Ba) by a solid-state metathesis approach. *Bull. Mater. Sci.* **2008**, *31*, 885−890.
(34) Cheng, J.; Alonso, J. A.; Suard, E.; Zhou, J.; Goodenough, J. B. A new perovskite polytype in the high-pressure sequence of $BaIrO_3$. *J. Am. Chem. Soc.* **2009**, *131*, 7461−7469.
(35) Jin, C. Q.; Zhou, J. S.; Goodenough, J. B.; Liu, Q. Q.; Zhao, J. G.; Yang, L. X.; Yu, Y.; Yu, R. C.; Katsura, T.; Shatskiy, A.; Ito, E. High-pressure synthesis of the cubic perovskite $BaRuO_3$ and evolution of ferromagnetism in $ARuO_3$ (A = Ca, Sr, Ba) ruthenates. *Proc. Natl. Acad. Sci. U. S. A.* **2008**, *105*, 7115−7119.
(36) Tsujimoto, Y.; Tassel, C.; Hayashi, N.; Watanabe, T.; Kageyama, H.; Yoshimura, K.; Takano, M.; Ceretti, M.; Ritter, C.; Paulus, W. Infinite-layer iron oxide with a square-planar coordination. *Nature* **2007**, *450*, 1062−1065.
(37) Yamamoto, T.; Kobayashi, Y.; Hayashi, N.; Tassel, C.; Saito, T.; Yamanaka, S.; Takano, M.; Ohoyama, K.; Shimakawa, Y.; Yoshimura, K.; Kageyama, H. $Sr_{1-x}Ba_x$) FeO_2 ($0.4 \leq x \leq 1$): a New Oxygen Deficient Perovskite Structure. *J. Am. Chem. Soc.* **2012**, *134*, 11444−11454.
(38) Rey, M.; Dehaudt, P.; Joubert, J.; Lambert-Andron, B.; Cyrot, M.; Cyrot-Lackmann, F. Preparation and structure of the compounds $SrVO_3$ and Sr_2VO_4. *J. Solid State Chem.* **1990**, *86*, 101−108.
(39) Brown, I. D.; Altermatt, D. Bond-valence parameters obtained from a systematic analysis of the inorganic crystal structure database. *Acta Crystallogr., Sect. B: Struct. Sci.* **1985**, *41*, 244−247.
(40) Brese, N.; O'keeffe, M. Bond-valence parameters for solids. *Acta Crystallogr., Sect. B: Struct. Sci.* **1991**, *47*, 192−197.
(41) Adkin, J. J.; Hayward, M. A. Structure and magnetism of 4H-$BaMnO_{3-x}$ ($0\leqslant x\leqslant 0.35$) and 4H-$Ba_{0.5}Sr_{0.5}MnO_{3-x}$ ($0\leqslant x\leqslant 0.21$). *J. Solid State Chem.* **2006**, *179*, 70−76.
(42) Mori, K.; Kamiyama, T.; Kobayashi, H.; Oikawa, K.; Otomo, T.; Ikeda, S. Structural Evidence for the Charge Disproportionation of Fe^{4+} in $BaFeO_{3-\delta}$. *J. Phys. Soc. Jpn.* **2003**, *72*, 2024−2028.
(43) Arévalo-López, A. M.; Attfield, J. P. High-pressure $BaCrO_3$ polytypes and the 5H−$BaCrO_{2.8}$ phase. *J. Solid State Chem.* **2015**, *232*, 236−240.
(44) Delattre, J. L.; Stacy, A. M.; Siegrist, T. Structure of ten-layer orthorhombic $Ba_5Fe_5O_{14}$ ($BaFeO_{2.8}$) determined from single crystal X-ray diffraction. *J. Solid State Chem.* **2004**, *177*, 928−935.
(45) Nakai, Y.; Iye, T.; Kitagawa, S.; Ishida, K.; Ikeda, H.; Kasahara, S.; Shishido, H.; Shibauchi, T.; Matsuda, Y.; Terashima, T. Unconventional superconductivity and antiferromagnetic quantum critical behavior in the isovalent-doped $BaFe2(As_{1-x}P_x)_2$. *Phys. Rev. Lett.* **2010**, *105*, 107003.
(46) Böhmer, A.; Arai, T.; Hardy, F.; Hattori, T.; Iye, T.; Wolf, T.; Löhneysen, H. v.; Ishida, K.; Meingast, C. Origin of the tetragonal-to-orthorhombic phase transition in FeSe: A combined thermodynamic and NMR study of nematicity. *Phys. Rev. Lett.* **2015**, *114*, 027001.
(47) Moriya, T. *Spin Fluctuations in Itinerant Electron Magnetism*; Springer-Verlag: Berlin, 1985.
(48) Kasahara, S.; Shibauchi, T.; Hashimoto, K.; Ikada, K.; Tonegawa, S.; Okazaki, R.; Shishido, H.; Ikeda, H.; Takeya, H.; Hirata, K.; Terashima, T.; Matsuda, Y. Evolution from non-Fermi-to Fermi-liquid transport via isovalent doping in $BaFe_2(As_{1-x}P_x)_2$ superconductors. *Phys. Rev. B: Condens. Matter Mater. Phys.* **2010**, *81*, 184519.
(49) Takeda, Y.; Kanamura, F.; Shimada, M.; Koizumi, M. The crystal structure of $BaNiO_3$. *Acta Crystallogr., Sect. B: Struct. Crystallogr. Cryst. Chem.* **1976**, *32*, 2464−2466.
(50) Chamberland, B.; Sleight, A.; Weiher, J. Preparation and characterization of $BaMnO_3$ and $SrMnO_3$ polytypes. *J. Solid State Chem.* **1970**, *1*, 506−511.
(51) Gonzalez-Calbet, J.; Parras, M.; Alonso, J.; Vallet-Reg1, M. Prediction of Novel $BaMnO_{3-y}$ ($0< y < 0.1$) Perovskite Related Phases. *J. Solid State Chem.* **1994**, *111*, 202−207.
(52) Overton, A. J.; Best, J. L.; Saratovsky, I.; Hayward, M. A. Influence of Topotactic Reduction on the Structure and Magnetism of the Multiferroic $YMnO_3$. *Chem. Mater.* **2009**, *21*, 4940−4948.

DOI: 10.1021/acs.chemmater.7b04571
Chem. Mater. 2018, 30, 1566−1574